NRC Research Press

ARTICLE

Scaling up experimental trawl impact results to fishery management scales — a modelling approach for a "hot time"

Nick Ellis, Francis Pantus, and C. Roland Pitcher

Abstract: Numerous studies have quantified trawl impacts at small scales. However, effective management of trawl impacts requires synthesis of experimental results (biomass depletion per tow and subsequent recovery) and application at fishery scales — realistically, this is achievable only in a modelling framework. We present a method for scaling up experimental results for management applications that incorporates a benthic biomass model having exponential trawl depletion and logistic recovery. Ultra-fine trawl-track data, supported by simulations, show that realistic trawling can be represented by a negative-binomial stochastic process, with intensity governed by large-scale effort and aggregation by a tunable parameter. Two mechanisms of the process are considered: aggregations in space (hot spots) and aggregations in time (hot times), which yields a logistic differential equation for the large-scale biomass over time. The model shows that scaling from fine scale to fishery scale depends on the degree of aggregation of fishing, with increasing aggregation lowering depletion rates at fishery scales. This model is a fundamental step in enabling assessment of large-scale implications and evaluating alternative management strategies.

Résumé : De nombreuses études ont quantifié les impacts des chaluts à de petites échelles. La gestion efficace des impacts des chaluts nécessite toutefois une synthèse des résultats expérimentaux (épuisement de la biomasse par trait et rétablissement subséquent) et son application à l'échelle de la pêche, ce qui ne peut raisonnablement être accompli que par modélisation. Nous présentons une méthode de mise à l'échelle des résultats expérimentaux pour des applications de gestion qui intègre un modèle de biomasse benthique avec épuisement associé au chalutage exponentiel et rétablissement logistique. Des données de résolution ultrafine relatives aux traces de chalut appuyées par des simulations montrent qu'un chalutage réaliste peut être représenté par un processus stochastique binomial négatif dans lequel l'intensité est régie par l'effort à grande échelle et la concentration par un paramètre ajustable. Deux mécanismes du processus sont examinés, les concentrations dans l'espace (points chauds) et les concentrations dans le temps (moments chauds), ce qui donne une équation différentielle logistique pour la biomasse à grande échelle en fonction du temps. Le modèle démontre que le passage d'une échelle fine à l'échelle de la pêche dépend du degré de concentration de l'activité de pêche, une plus grande concentration se traduisant par une réduction des taux d'épuisement à l'échelle de la pêche. Ce modèle constitue une étape fondamentale dans l'évaluation des conséquences à grande échelle et de différentes stratégies de gestion. [Traduit par la Rédaction]

Introduction

Seabed trawling is a large-scale activity conducted over as much as 75% of the world's continental shelves at varying levels of density (F. Pantus, unpublished data, in Kaiser et al. 2002) and has been attributed a range of direct impacts and other effects (see, e.g., Jennings and Kaiser (1998) for a review of the extensive literature). As countries progress toward ecosystem-based approaches to management, trawl fisheries are under increasing pressure to manage the wider environmental effects of their activities.

The results of scientific studies on the effects of trawling are highly variable. Collie et al. (2000), using a meta-analysis of dozens of studies, have shown that the extent of trawl impacts are dependent on habitat type, benthic composition, trawl intensity, and trawl gear types. Such diversity of effects has been reaffirmed by Kaiser et al. (2006) and Pitcher et al. (2009). Variation over most of the above factors may be present within the larger scale of a fishery jurisdiction, making understanding of the regional effects complex and management choices difficult. Fewer studies have attempted to measure recovery rates (e.g., van Dolah 1987; Kaiser et al. 1998; Tuck et al. 1998; Kenchington et al. 2006; for trawling on epifauna), particularly for vulnerable longer-lived fauna (Sainsbury et al. 1997; Pitcher et al. 2008).

Larger-scale empirical studies (~10s–100s km) have typically attempted to compare trawled areas with untrawled areas (e.g., Sainsbury et al. 1992; Collie et al. 1997; McConnaughey et al. 2000; Burridge et al. 2006) and, pseudoreplication and (or) confounding aside, these may or may not have shown quantitative differences between such areas. However, the natural dynamics and exploitation history of these areas generally is not known sufficiently to understand the processes that have led to any measured differences in state. It is therefore difficult for managers to make direct use of such (effectively qualitative) information for anticipating the consequences of future management actions. Small-scale studies, on the other hand, have typically conducted experiments to make quantitative measurements of direct removal or mortality rates (Bergman and van Santbrink 2000; Moran and Stephenson 2000; Hansson et al. 2000; Burridge et al. 2003) at the scale of the trawl gear (<1–10 km) under controlled "exploitation". Here, while the direct impact process may be better understood, the implications of such results are difficult to apply at space and time scales relevant to management.

Received 6 August 2013. Accepted 8 January 2014.

Paper handled by Associate Editor Terrance Quinn II.

N. Ellis and C.R. Pitcher. CSIRO Wealth from Oceans Flagship, Ecosciences Precinct, 41 Boggo Road, Dutton Park, Queensland, Australia.
F. Pantus. Australian Rivers Institute, Griffith University, Brisbane, Australia.
Corresponding author: Nick Ellis (e-mail: nick.ellis@csiro.au).

Consequently, there is a need to scale up the effects of trawling inferred from such experiments to effects at the fishery scale in a way that takes into account — initially at least — the impact process, benthic dynamics, and trawl effort intensity. Such a link between small and large scales could not only shed light on large-scale study results, but would be a valuable tool to assist with evaluation of alternative management strategies.

A key input to this scaling-up process is data on the spatial and temporal distribution of trawling intensity. It is well-known that trawling is aggregated, since fishers go preferentially to areas with better catches. However, it is important to realize that the aggregation occurs not only at fishery scales but also at the fine scale of the trawl gear (Rijnsdorp et al. 1998; Pitcher et al. 2000). Moreover, Pitcher et al. (2000) showed that the overall impact of aggregated trawling within an area was substantially less than the impact caused by the same amount of trawling swept uniformly over that area. It is therefore crucial to adequately describe aggregation at such fine scales.

Unfortunately it is challenging to obtain data at this fine scale. Vessel tracks are routinely recorded using geographic positioning system (GPS) plotters, but they are usually treated as commercial in confidence and so unavailable. Some fisheries require shot-by-shot logging, but this provides only a coarse pointwise summary of a trawling process that is extended over space and time. Vessel monitoring systems (VMS), which are chiefly used by management as a compliance tool, provide exact positions at regular (e.g., 2 h) polling frequencies. Subsequent processing, such as interpolation or spreading with a spatial kernel, results in an estimated trawling distribution that is typically gridded at 1 n.mi. (1 n.mi. = 1.852 km) resolution, depending on the polling frequency (see review of methods in Lee et al. 2010). Logbooks are the most widely available data; however, they provide the trawling distribution at the coarsest resolution of a management grid cell (typically ~6 n.mi. or larger, hereafter referred to as a "grid"). With the exception of the unavailable GPS tracks, none of these data provide the trawl distribution at the scale of the gear tracks over the ground.

A few authors have attempted to scale up impacts from experimental scale to fishery scale. Piet et al (2000) converted Dutch beam trawl effort reported at 30 n.mi. resolution into a fine-scale pattern at 1 n.mi. resolution, using the distribution estimated by Rijnsdorp et al. (1998) from GPS data on a representative sample (13%) of the fleet. Assuming that effort was uniform within each 1 n.mi. grid, Piet et al. (2000) estimated annual mortality given a heterogeneous biomass distribution. Bergman and van Santbrink (2000) also provided mortality estimates using a coarser 10 n.mi. grid.

Both of these authors relied on the assumption of uniform subgrid effort, which tends to overestimate the impact. Alternatively, Pitcher et al. (2000) estimated the distribution of effort on an ultra-fine grid of 30 m squares (referred to here as "pixels"), comparable with the scale of the gear. Working with Australian east coast trawl fishery logbook data collected on a 6 n.mi. grid, they employed a fractal assumption that the distribution of effort among 30 m pixels within each 6 n.mi. grid was the same as the distribution of effort among 6 n.mi. grids within the whole fishery, to estimate regional-scale implications. Here, we adapt this idea by replacing the empirical approach with a formal probability distribution.

This paper describes the initial development of a dynamic model that incorporates impact, recovery, and fleet dynamics and provides a method to link between small-scale impacts and large-scale implications by expressing the effects of trawling on benthic biota as a stochastic process. The intensity of the process is governed by the known trawl effort at the level of the management grid, and the degree of within-grid aggregation of the distribution is given by a single tunable parameter. We show that this simple model of exponential trawl depletion and logistic recovery, with parameters measurable by small-scale experiments, when combined with a stochastic trawling process, scales up to yield a logistic differential equation for biomass at the scale of the management grid. We also show how the tunable aggregation parameter, which is directly related to Rijnsdorp et al.'s (1998) "patchiness", can be estimated from submanagement-grid information, such as GPS position records, vessel monitoring data, or simulation.

The model and its components

The purpose of the modelling presented here is to convert impacts occurring at the pixel scale, and understood through experimental data at the same scale, into impacts at the grid scale for use by management. The first step is to derive a biomass model that takes both depletion by trawling and biological growth into account.

Our dynamic model for biomass $B(t)$ of a benthic taxon undergoing depletion by and recovery from trawling is given by the differential equation

$$\frac{dB}{dt} = RB(t)\,[1 - B(t)/K] - DE(t)B(t) \quad (1)$$

It is a Schaefer-type differential equation (Schaefer 1954) with logistic growth term proportional to recovery rate R and removal term proportional to depletion rate D and fishing effort rate E. This model operates on the scale of the management grid and arises from the aggregation of depletion and recovery processes operating on the scale of the trawl gear. These small-scale processes are scaled up to result in the differential equation describing on-the-ground impacts in terms of management-scale effort records. The model is illustrated schematically in Fig. 1, and the scaling-up method and derivation of eq. 1 are described in the section "Scaling up from pixel to grid scale".

Grid- and pixel-scale distribution of effort

There are several scales at which trawling impacts can be described, but this paper focuses on two: the (larger, management) grid scale and the (smaller, gear) pixel scale. The grid scale refers to the scale of the management grid, on which effort is reported in logbooks in most fisheries. The grid, typically squares with sides of approximately 10–100 km, is the smallest convenient scale on which to report impacts that are relevant to management. The pixel scale refers to the scale at which the direct impacts occur through interaction of biota with the trawl gear. Estimates of depletion and recovery rates from trawling manipulation experiments are measured on this pixel scale. The actual pixel size depends on the width of the gear; for trawling, squares with sides of 10–100 m are appropriate.

We use the term "coverage" to quantify the amount of trawl effort at both pixel and grid scales. At the pixel scale, coverage is the (integer) number of trawl passes over the pixel; at the grid scale, coverage is the ratio of total swept area to grid area. The grid coverage is therefore the mean coverage over all pixels within the grid.

To express the trawl effort at the pixel scale, we assume a probability distribution $P_t(n)$ for the cumulative number of trawl passes n over pixels within a grid after time t. The mean $\mu(t)$ is the cumulative coverage. Its derivative $d\mu/dt \equiv E(t)$ is the instantaneous effort rate (i.e., the coverage per unit time) that can be sourced from grid-scale data such as log books. The distribution $P_t(n)$ can be calibrated using a combination of trawl track data and simulation (see section on "Validation and calibration").

Although the following arguments apply for a general $P_t(n)$, it is useful to concentrate on a particular distribution that can accommodate both the degree of aggregation and the level of trawl coverage as the trawl effort accumulates over time. We therefore

Fig. 1. Schematic diagram of the components of the biomass differential equation at the grid scale. Components are either measured at the grid scale (*K*, *B*, *E*) or derived (*D*, *R*) by scaling up experimental data at the pixel scale (*d*, *r*) assuming a degree of trawl aggregation (β).

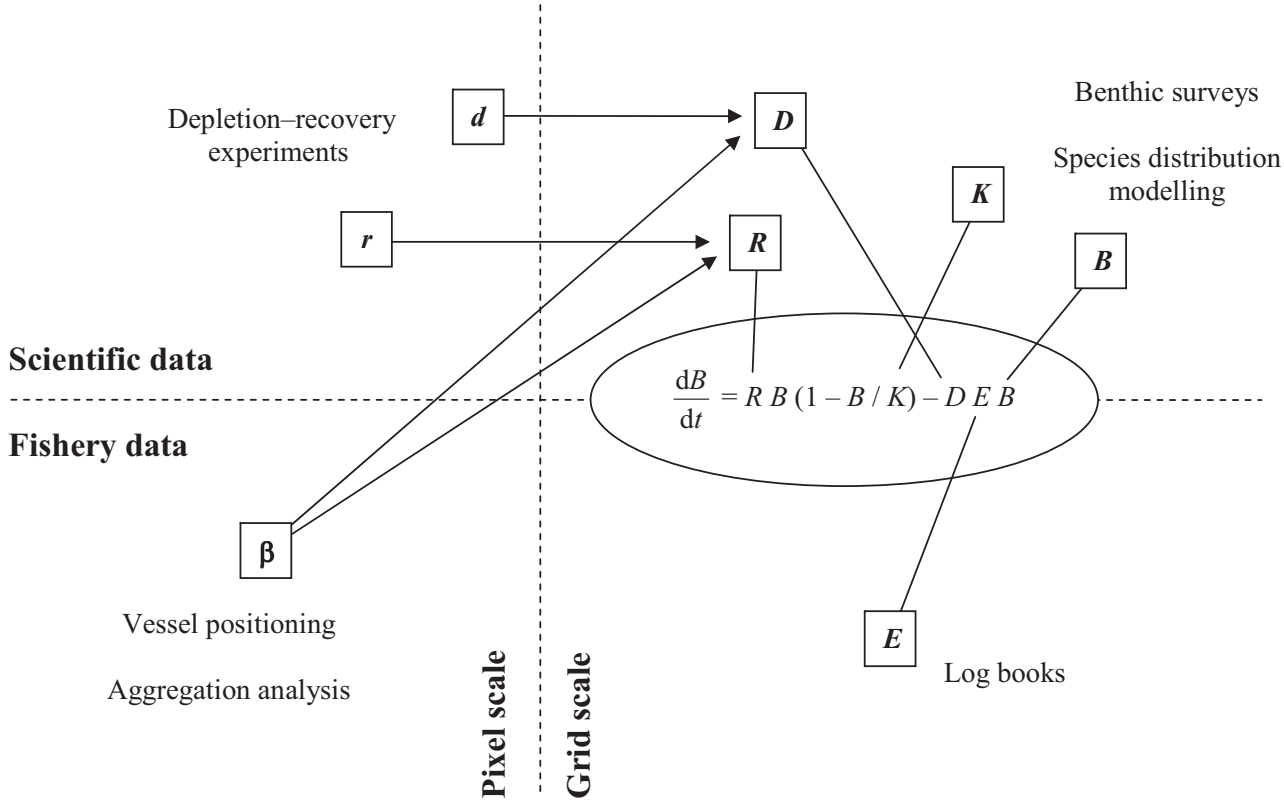

use the negative binomial distribution (NBD; Gurland 1959), it being the best-known distribution for describing count data arising from an aggregated process. The NBD has two parameters: the mean μ and an aggregation parameter β. The greater the degree of aggregation, the larger the value of β. The probability of n trawl passes over a pixel given these parameters is

$$(2)\qquad P(n|\mu,\beta) = \frac{\Gamma(\mu/\beta + n)}{n!\Gamma(\mu/\beta)}\left(\frac{\beta}{\beta+1}\right)^n\left(\frac{1}{\beta+1}\right)^{\mu/\beta}$$

(This is Gurland's eq. 5 with his parameters (k, p) replaced by (μ/β, β).) The NBD includes the Poisson distribution as a special case ($\beta = 0$; it can be shown that $\lim_{\beta\to 0} P(n|\mu,\beta) = \mu^n e^{-\mu}/n!$, the Poisson probability), which arises when trawling is completely random. When $\beta < 0$, the distribution describes patterns that exhibit some regularity, with complete regularity occurring when $\beta = -1$. Furthermore, when μ/β is a negative integer, the distribution becomes binomial. In aggregated patterns the variance exceeds the mean, whereas in regular patterns the variance is less than the mean; for completely random patterns the variance equals the mean.

Figure 2 shows three simulated trawl patterns on a 4 km × 4 km grid and corresponding histograms of spatial coverage. (See Supplementary Materials[1] for details on the trawl pattern simulator.) The mean coverage is the same in each case ($\mu = 0.51$), but the degree of aggregation varies. Fitting the negative binomial family to these histograms using the method of moments (eq. 13 in Gurland 1959) results in close agreement with these simulated results; the top case (Regular) is binomial with $\beta = -0.51$, the middle (Random) is Poisson with $\beta = 0$, and the bottom (Aggregated) is negative binomial with $\beta = 1.24$.

Trawling can be aggregated either spatially (hot spots) or temporally (hot times), and both mechanisms can be modelled by the NBD. Either mechanism is plausible for describing actual trawling; the hot spot mechanism describes persistent spatial aggregations, whereas the hot time mechanism captures behaviour where the trawler makes repeated passes over the same track in a short period of time.

In the hot spot mechanism, trawling occurs randomly within spatial patches, but the intensity per patch varies according to a Gamma distribution with mean μ and shape parameter μ/β. In the hot time mechanism, trawling "events" occur completely at random in space but are distributed in time according to an inhomogeneous random process, with probability of an event occurring within the infinitesimal time interval (t, $t + dt$) equal to $\beta^{-1}\log(1 + \beta)E(t)dt$. The temporal aggregation comes about by having the number of tows k per event distributed according to the logarithmic distribution $P(k) = [\beta/(\beta + 1)]^k/[k\log(1 + \beta)]$. This mechanism is an inhomogeneous Poisson point process with multiplicities (Cox and Isham 1980). The distributions for the number of tow passes per pixel after time t resulting from either mechanism (Poisson–Gamma mixture for the hot spots and Poisson–logarithmic compound for the hot times) are both NBD with parameters μ and β (Quenouille 1949; Eaton and Fortin 1978; Diggle and Milne 1983). An example of each mechanism is shown in Fig. 3. In each case the total number of tows after 10 years has NBD with $\mu = 30$ and $\beta = 1$.

The hot spot mechanism may be in effect in places where the trawl grounds are limited by geomorphology, such as spawning aggregations on seamounts or close to the edge of untrawlable

[1]Supplementary data are available with the article through the journal Web site at http://nrcresearchpress.com/doi/suppl/10.1139/cjfas-2013-0426.

Fig. 2. Simulated trawl coverage patterns and corresponding histograms (pixel counts) of coverage. The pattern at the top is regular trawling, at the middle is random trawling, and at the bottom is aggregated trawling. The mean coverage in each case is $\mu = 0.51$. The histograms follow binomial, Poisson, and negative binomial distributions, respectively. Trawl tracks are drawn over the regular pattern to suggest how the pattern arose.

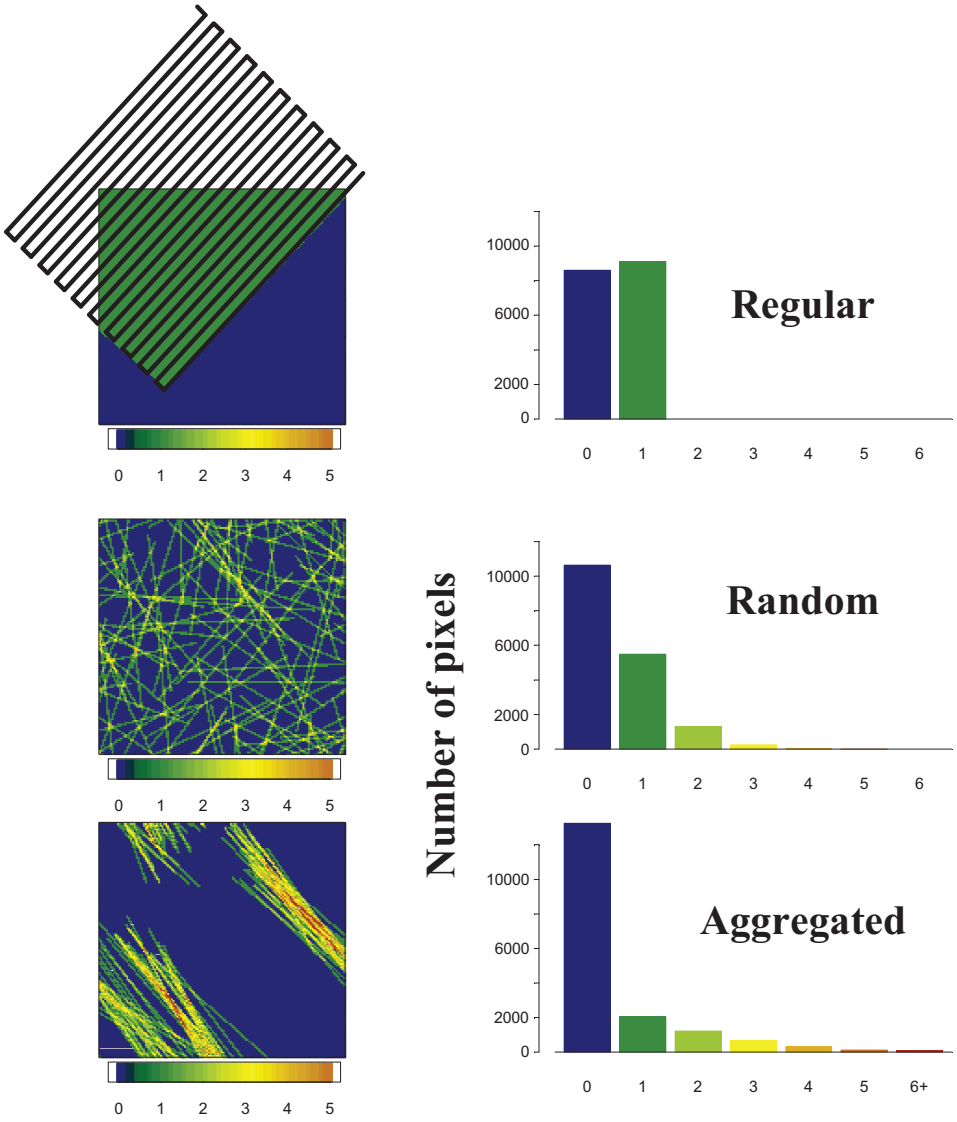

ground, particularly if the topography channels the trawl shots into "runways". Evidence for persistent trawling hot spots tends to be anecdotal, however, and may be difficult to obtain owing to constraints of confidentiality. Piet and Quirijns (2009) showed that coarse-scale spatial patterns of Dutch beam trawlers are correlated from one year to the next, but that the correlation became much weaker at finer scales. The patterns gradually shifted over time so that over the long term the pattern was spatially random. On the other hand, a study by Rijnsdorp et al. (2011) on the same fleet observed repeated-tow patterns within patches of trawling, which may support the hot time mechanism.

It transpires that the process of scaling up to the grid scale is tractable only for the hot time mechanism. Therefore, the remainder of the methods and results (sections "Scaling up from pixel to grid scale" and "Validation and calibration") assumes hot times, and we defer consideration of the hot spot mechanism to the Discussion. Further, we assume that the time-varying properties of the hot time trawling distribution are captured by $\mu(t)$, so that β is constant. See the Supplementary Materials[1] for a simulation to check the plausibility of this assumption. Nevertheless, the fixed-β assumption can be relaxed; see Appendix B.

The probability generating function (pgf) for the number of tows after time t is

$$(3) \qquad g_t(z) = [1 + \beta(1 - z)]^{-\mu(t)/\beta}$$

The variance–mean relationship is

$$(4) \qquad V(t) = \mu(t)(1 + \beta)$$

(i.e., the variance is proportional to the mean). This relationship demonstrates how the parameter β quantifies the degree of aggregation, since the factor $1 + \beta$ is the overdispersion relative to the Poisson case. Such overdispersion is seen in trawl-coverage distributions (Rijnsdorp et al. 1998). The quantity $1 + \beta$ is the same as Rijnsdorp et al.'s (1998) coefficient of patchiness C.

Fig. 3. Comparison of (left panel) hot spot and (right panel) hot time processes for a taxon with $d = 0.1$ and $r = 0.3$ in 10 pixels within a grid having constant coverage rate $E(t) = 3.0$. Each horizontal strip shows the relative biomass trajectory (solid line) in a single pixel. Vertical ticks denote trawling events with length proportional to number of tows (between 1 and 10). Each strip is labelled at right by the expected annual trawl intensity, which for the hot spot process varies among pixels. The mean across each of the 10 pixels is denoted by a dashed line. Pixels are sorted on the total number of tows.

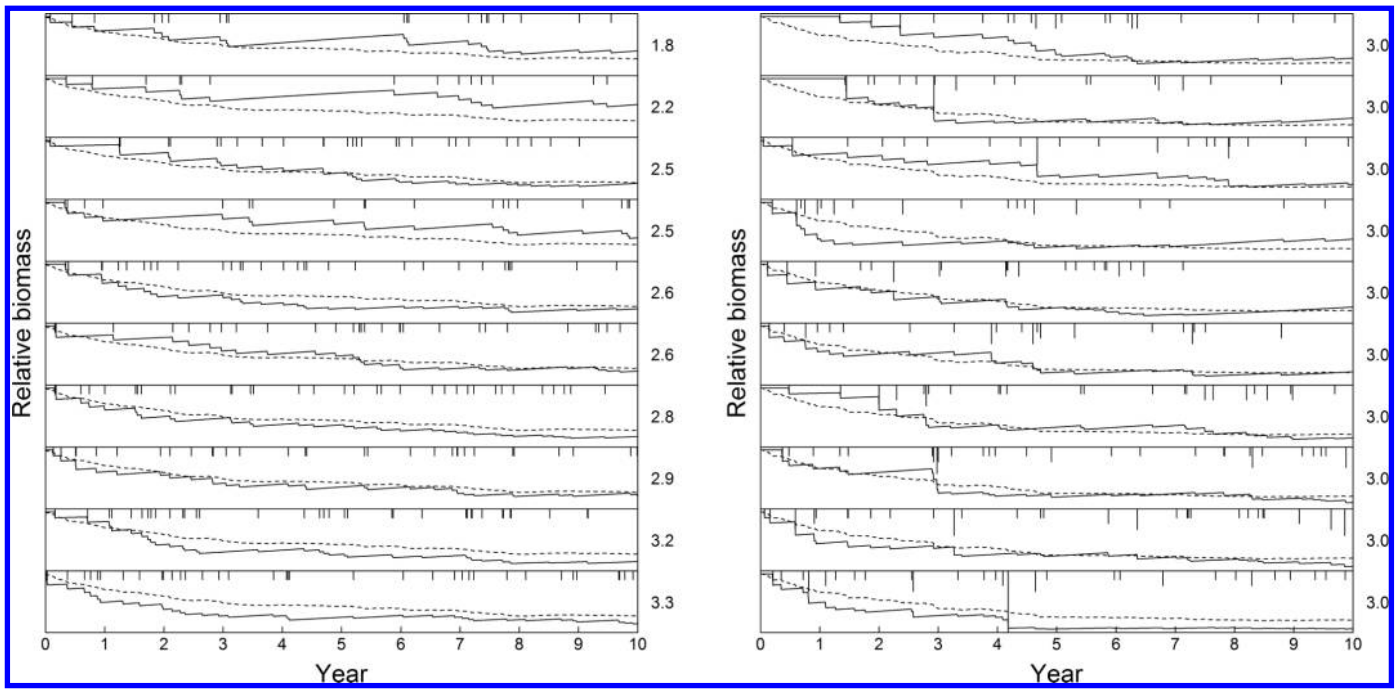

Grid-scale pristine biomass distribution

It is well-known that the grid-scale equation (eq. 1) can be solved for relative biomass $b = B/K$ under the assumption that the pristine (or before impact) biomass is at carrying capacity ($B(0) = K$), since then $b(0) = 1$, and $b(t)$ can be calculated for all $t > 0$ given R, D, and $E(t)$. Our model makes this assumption and allows $B(0)$ to vary from grid to grid. The pixel-scale pristine biomass, however, is only specified to the extent that the biomass density $\rho(\boldsymbol{x})$ at pixel $\boldsymbol{x}$ satisfies $B(0) = \int_A \rho(\boldsymbol{x})\mathrm{d}A$, where A is the area of the grid.

The model was originally designed for data-poor applications where all assessments were in terms of relative biomass, because K was unknown. In the past decade, however, considerable research has been carried out to map species distributions on the seabed (e.g., Pitcher et al. 2007*a*), making it feasible in principle to estimate K and, hence, absolute biomass $B(t)$ for all t.

Pixel-scale impact model

To estimate some of the parameters of the model, information on the depletion of biomass within a pixel trawled one or more times is provided by trawling experiments. In the experiment by Poiner et al. (1998) in the northern section of the Great Barrier Reef (GBR), strips of seabed were repeatedly trawled 13 times, and the amount of biomass removed per taxon was recorded. These authors, assuming that a fixed proportion d of the biomass was removed by each tow, provided estimates of d. Burridge et al. (2003), allowing d to be a random variable, estimated its mean and variance for various taxa. Here we make the fixed-proportion assumption of Poiner et al. (1998); that is, if the initial biomass of a particular taxon is $B^{(0)}$ in some area within the trawl path, then after n tows with depletion rate d, the remaining biomass $B^{(n)}$ satisfies

$$B^{(n)} = (1 - d)^n B^{(0)} \tag{5}$$

This is a conservative assumption, since the amount of depletion is maximized under fixed d compared with the case when d is a random variable (see Appendix A).

Results from the repeat-trawl experiment (Fig. 4) show the estimated biomass of gorgonians and sponges remaining along a particular track after 0 to 13 tows. The depletion rates for the two species are quite different, yet both conform closely to the fixed-proportion depletion model ($R^2 = 0.97$ and 0.99, respectively).

Pixel-scale recovery model

Within a pixel, biomass B is assumed to recover from trawling impacts according to the logistic recovery equation

$$\frac{\mathrm{d}B}{\mathrm{d}t} = rB(t)[1 - B(t)/K] \tag{6}$$

where K is the carrying capacity of the pixel, and r is the pixel-scale recovery rate. It is convenient to work with relative biomass $b(t) \equiv B(t)/K$. The relative biomass is bounded between 0 and 1 and takes its maximum value when the biomass reaches the carrying capacity. The biomass undergoes discrete (possibly multiple) trawl events, occurring at random times and each removing a fixed proportion d of the biomass. Suppose that a depletion event occurs at time t_0, leaving a relative biomass $b(t_0)$. Then at later time t, the relative biomass is

$$b(t) = \frac{b(t_0)\mathrm{e}^{r(t-t_0)}}{1 + b(t_0)[\mathrm{e}^{r(t-t_0)} - 1]} \tag{7}$$

which is the solution of eq. 6.

The pixel-scale recovery rate captures the increase in biomass due to intrinsic growth and local recruitment; it is this quantity that could be measured by a fine-scale depletion–recovery exper-

Fig. 4. Estimated biomass during a series of trawls for (left panel) gorgonians and (right panel) sponges from the CSIRO–QDAFF (Queensland Department of Agriculture, Fisheries and Forestry) experiment in the far north of the Great Barrier Reef (Poiner et al. 1998).

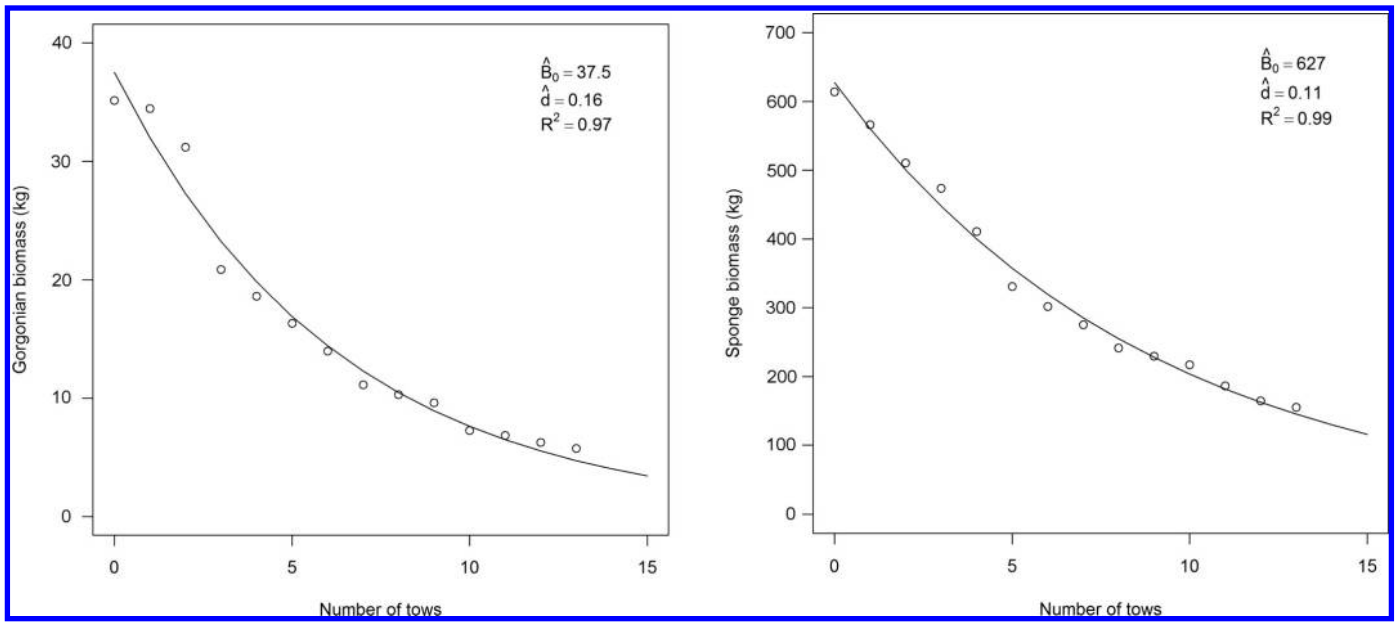

iment. Implicit in this model is that pixels are independent of one another. This assumption is suitable for taxa with asexual propagules of larvae having short-range dispersal relative to the pixel size, such as the sessile fauna considered here. For mobile taxa or sessile taxa with longer-range larval dispersal, the recovery model would need to include extra parameters describing recruitment or migration from neighbouring or distant pixels.

Scaling up from pixel to grid scale

To clarify the effect of the trawl coverage distribution P_t, the section "Depletion without recovery" derives a formula for grid-scale biomass at time t under depletion, ignoring recovery. In the section "Depletion with recovery", the recovery component is incorporated to yield a differential equation for grid-scale biomass.

Depletion without recovery

The remaining biomass $B(t)$ over the entire grid is given (in the limit of infinitesimal pixels) by the following integral

$$B(t) = \int_A \rho(\boldsymbol{x})(1-d)^{n_t(\boldsymbol{x})}\mathrm{d}^2\boldsymbol{x} \tag{8}$$

where $n_t(\boldsymbol{x})$ is the coverage at $\boldsymbol{x}$ after time t, $\mathrm{d}^2\boldsymbol{x}$ is an infinitesimal area element, and the integration is over the area of the grid A. Both $\rho(\boldsymbol{x})$ and $n_t(\boldsymbol{x})$ are random variables. Let $A_t(k) \equiv \{\boldsymbol{x}: n_t(\boldsymbol{x}) = k\}$ be the (usually disjoint) area covered k times at time t. Then, since the depletion rate d is constant:

$$B(t) = \sum_{k=0}^{\infty}\left[(1-d)^k \int_{A_t(k)} \rho(\boldsymbol{x})\mathrm{d}^2\boldsymbol{x}\right] \tag{9}$$

(See Appendix A for the case where d is not fixed.) The expected value of $A_t(k)$ (with respect to the random trawling process) is the expected proportion of A covered k times, thus:

$$\mathbf{E}[A_t(k)] = P_t(k)A \tag{10}$$

(Please note that the expectation symbol **E** is not to be confused with the effort rate E.).

We next make the important assumption that the distribution of trawling is independent of the distribution of initial biomass. This is consistent with the hot time mechanism but **not** with the hot spot mechanism (since target areas may also be hot spots in biomass). Given independence, the expectation can be moved inside the integral, thus:

$$\mathbf{E}\left[\int_{A_t(k)} \rho(\boldsymbol{x})\mathrm{d}^2\boldsymbol{x}\right] = \int_{A_t(k)} \mathbf{E}[\rho(\boldsymbol{x})]\mathrm{d}^2\boldsymbol{x} = P_t(k)A\mathbf{E}[\rho] = P_t(k)\mathbf{E}[B(0)] \tag{11}$$

and therefore, from eq. 9,

$$\mathbf{E}[B(t)] = \sum_{k=0}^{\infty}(1-d)^k P_t(k)\mathbf{E}[B(0)] \tag{12}$$

This last expression relates the expected biomass at time t to the expected initial biomass through the pgf of the coverage distribution, $g_t(z) \equiv \sum_{k=0}^{\infty} z^k P_t(k)$, so that

$$\mathbf{E}[B(t)] = g_t(1-d)\mathbf{E}[B(0)] \tag{13}$$

This equation states that the proportion of biomass remaining at time t is $g_t(1-d)$. Because the area of a grid is much larger than that of a single trawl, it follows that, by the central limit theorem, the actual total biomass will be close to the expected total biomass. Therefore, from now on we drop the expectation symbol.

Equation 13 holds for a general distribution P_t. Specializing to the NBD, from eq. 3, the biomass is given by

$$B(t) = \exp[-D\mu(t)]B(0) \tag{14}$$

where

$$D = \log(1 + \beta d)/\beta \quad (15)$$

The quantity D is interpreted as the grid-scale fractional depletion rate per unit effort rate; it is the grid-scale analogue of d. For aggregated trawling ($\beta > 0$), D is less than d; for trawling exhibiting some regularity (i.e., $\beta < 0$), D is greater than d; and for random trawling with a Poisson distribution ($\beta = 0$), then $D = d$. This result accords with our expectation that higher aggregation has less impact, because subsequent tows cover ground that has already been depleted. Previous authors (Sainsbury et al. 1997; Poiner et al. 1998) have used the small-scale depletion rate to model depletion over the large scale. This result shows that the use of d is only justified when trawling is random. Equation 15 provides the link between pixel-scale and grid-scale depletion rates, taking into account the degree of aggregation.

Differentiating eq. 14 yields the dynamic equation for biomass:

$$\frac{dB}{dt} = -DE(t)B(t) \quad (16)$$

Note that whereas d describes a **discrete** depletion event (a tow), D describes a **continuous** process of depletion that arises from averaging over many discrete small-scale depletion events governed by d. In other words, d and D are depletion rates for, respectively, discrete and continuous units of effort.

Depletion with recovery

The differential equation for the grid-scale biomass is derived by computing the expected difference in biomass over a time interval Δt and taking the limit $\Delta t \to 0$. Consider the relative biomass b in a pixel $\boldsymbol{x}$. The relative biomass at time $t + \Delta t$ in terms of the biomass at time t is

$$b(t + \Delta t) = b(t)\{1 + r\Delta t[1 - b(t)]\}(1 - d)^{n(\Delta t)} + O(\Delta t^2) \quad (17)$$

(The order notation $O(\Delta t^2)$ indicates terms that can be ignored relative to the other terms on the right-hand side in the limit $\Delta t \to 0$.) This can be partially derived from eq. 7 by substituting $(t + \Delta t, t)$ for (t, t_0) and expanding out up to terms linear in Δt. The factor $(1 - d)^{n(\Delta t)}$ involving d is the stochastic depletion, where the random variable $n(\Delta t)$ is the number of trawl passes over $\boldsymbol{x}$ during the time interval $(t, t + \Delta t)$.

To find the expected relative biomass over the grid, we need to take two expectations: first, over the time interval $(t, t + \Delta t)$ for the trawling process; and second, over all pixels $\boldsymbol{x}$. Under the assumption that the trawl process during $(t, t + \Delta t)$ is independent of the process before time t and that the process is spatially homogeneous, we may take expectations of the trawling independently of the relative biomass.

From eq. 3

$$\mathbf{E}[(1 - d)^{n(\Delta t)}] = g_{\Delta t}(1 - d) = 1 - DE(t)\Delta t + O(\Delta t^2) \quad (18)$$

where $E(t)$ is the effort rate and D is given by eq. 15. Taking expectations over all pixels $\boldsymbol{x}$, we find

$$\mathbf{E}[b(t + \Delta t)] = \mathbf{E}[b(t)] + \Delta t\big(r\{\mathbf{E}[b(t)] - \mathbf{E}[b(t)^2]\} - DE(t)\mathbf{E}[b(t)]\big) + O(\Delta t^2) \quad (19)$$

Setting mean $\bar{b}(t) \equiv \mathbf{E}[b(t)]$ and variance $V(t) \equiv \mathrm{Var}[b(t)] = \mathbf{E}[b^2] - (\mathbf{E}[b])^2$ and taking the limit of $\Delta\bar{b}/\Delta t$ as $\Delta t \to 0$ yields

$$\frac{d\bar{b}}{dt} = r\bar{b}(t)[1 - \bar{b}(t)] - DE(t)\bar{b}(t) - rV(t) \quad (20)$$

This is a differential equation for the grid-scale mean biomass in terms of small-scale parameters r and d and aggregation parameter β (the last two through D). The first term on the right-hand side is the classic recovery term with rate equal to the pixel-scale recovery rate. The second term is the depletion term that was derived in the last section. The third term effectively reduces the recovery at the grid scale.

Because $\bar{b}$ is bounded, its variance cannot exceed $\bar{b}(1 - \bar{b})$, so $V = \phi\bar{b}(1 - \bar{b})$, where $\phi \in [0, 1]$ depends on time. Then eq. 20 becomes

$$\frac{d\bar{b}}{dt} = R(t)\bar{b}(t)[1 - \bar{b}(t)] - DE(t)\bar{b}(t) \quad (21)$$

where the grid-scale recovery rate $R(t) = r[1 - \phi(t)]$.

The quantity $\phi(t)$ depends on the distribution of the relative biomass, which in turn depends on the detailed history of depletion at every pixel. In practice, such details would not be available. Therefore, to obtain a large-scale equation for biomass that depends on only the statistics of the effort distribution but not on its actual details, we make the simplifying assumption: $\phi(t) = \phi_0$, a constant. This assumption is reasonable, because, as Appendix C shows, when $E(t)$ is constant, ϕ_0 does not depend on the value of $E(t)$; this suggests that $\phi(t)$ is only weakly dependent on $E(t)$ and hence on t. This variance–mean assumption $V(\mu) = \phi_0\mu(1 - \mu)$ is also commonly made in quasilikelihood estimation using generalized linear models with the binomial family (see, e.g., Venables and Ripley 2002). The validity of this assumption is tested using simulation in the next section, "Validation and calibration".

The grid-scale recovery rate $R(t)$ becomes constant and satisfies

$$R = r\log(1 + \beta d)/[-\beta\log(1 - d)] \quad (22)$$

See Appendix C for the derivation. For uniform trawling ($\beta = -1$), the grid is effectively a very large pixel, so that $R = r$. In general, though, the effect of subgrid trawling structure is to reduce the overall recovery rate (i.e., $R \le r$). Reintroducing the biomass B and carrying capacity K for the entire grid yields eq. 1.

Validation and calibration

The derivation of eq. 1 relies on the variance–mean assumption in the section "Depletion with recovery". We checked this directly by simulating a negative binomial trawling process at the pixel level and aggregating to the grid (see section "Testing the grid-scale depletion–recovery differential equation"). This method assumes that aggregation is generated by the hot time mechanism. We investigated the plausibility of this assumption by simulating the kind of aggregated trawling behaviour typical for the Australian east coast trawl fishery and capturing the pixel-level distribution over time. It was found that $V(t)$ was linear in $\mu(t)$, consistent with eq. 4 and the hot time assumption; see Supplementary Materials[1]. To calibrate the model for application to a real fishery, vessel-tracking data from the Australian Northern Prawn Fishery were examined. The validity of the NBD assumption was checked, and a range of realistic values for β was obtained (see section "Calibration from fine-scale effort data").

Testing the grid-scale depletion–recovery differential equation

To check that the grid-scale depletion–recovery equation accurately reproduces the grid-scale change in biomass, we simulated the detailed process of depletion and recovery at the pixel scale and aggregated the results up to the grid scale. Simulations were carried out as follows:

1. Partition the grid into a large number N of equal pixels and set the (relative) biomass to 1 in each pixel.

Fig. 5. Time series of annual effort, in units of coverage per year, for case (c) of the simulation in the section "Testing the grid-scale depletion–recovery differential equation". The coverage values were randomly generated from a lognormal distribution with mean 0.84 and variance 0.6, which is typical of reasonably heavily trawled grids in the East Coast Trawl Fishery.

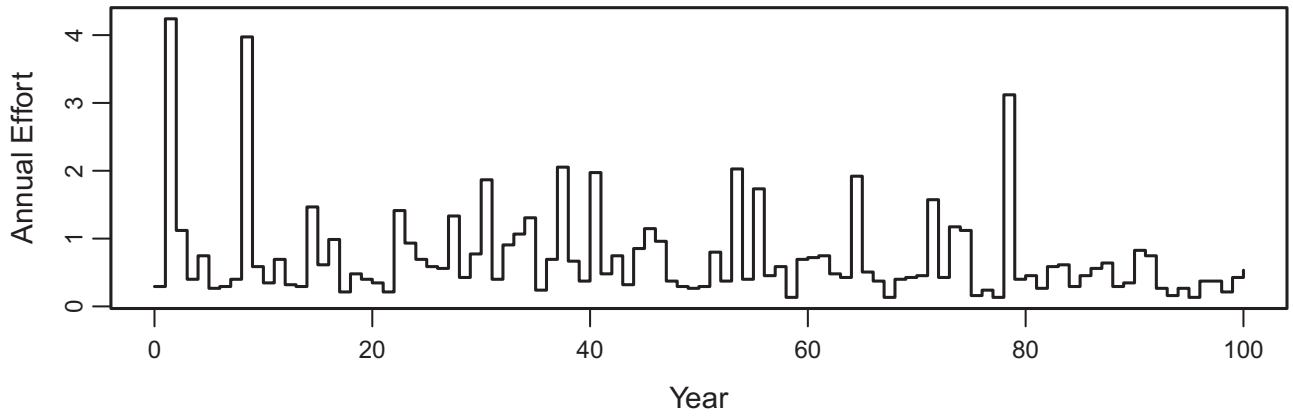

2. For each pixel $i = 1, ..., N$, sample the number of tows n_i within a certain time step Δt. This is done by sampling first the number of "events" (usually 0 or 1) from the Poisson distribution and then the number of tows per event from the logarithmic series distribution, following the hot time mechanism (refer to section "Grid- and pixel-scale distribution of effort").
3. Deplete the biomass by factor $(1 - d)^{n_i}$ and allow it to recover for time Δt along the logistic curve (eq. 17) using the exact form in eq. 7.
4. At each time t compute the mean $b(t)$ and variance $V(t)$ of the remaining relative biomass across all pixels. Figure 3 (right panel) illustrates this procedure for $N = 10$ pixels.

We considered three cases: case (a): recovery $r = 0.11$ and constant effort rate $E(t) = 1$; case (b): $r = 0.3$ and $E(t) = 1$; and case (c): $r = 0.11$ and time-varying $E(t)$ randomly generated from a lognormal distribution with mean 0.84 and variance 0.6. For each case we used two values of depletion ($d = (0.1, 0.3)$), resulting in six parameter combinations altogether. The aggregation parameter was set at $\beta = 5$. For each combination, three simulations were run using $N = 1000$ pixels and a time step $\Delta t = 0.1$ years; $b(t)$ and $V(t)$ were recorded at $t = 0, 1, \ldots, 100$ years.

We chose the properties of the effort pattern in case (c) to be representative of fairly heavily trawled grids in the Queensland East Coast Fishery. From the fleet's logbook data for the period 1993–1997, the 80th percentile of time-averaged effort in a 6 min grid was 67 boat days per year. Assuming average boat characteristics (28 m sweep, 3 knot tow speed (1 kn = 1.852 km·h^{-1}), and 10 h trawling per day), this effort translates to a coverage of 0.84. We estimated the between-year variance by pooling the effort from 20 grids around the 80th percentile, taking logs, finding the sample variance, and back-transforming to get the variance on the original scale. A series of effort rates $E(t)$ was created by taking independent samples from this distribution. This is plotted in Fig. 5.

The results are shown in Fig. 6. The agreement between the simulations and the model is quite satisfactory (left-hand column). The model is unbiased in the steady state (see case (b), $d = 0.1$) as expected. When the biomass is not constant, the model slightly underestimates it. This bias is most marked for case (b) with $d = 0.3$. In this case, the large-scale recovery and depletion rates balance almost exactly, and so the decay to the steady state (zero biomass) is very slow (i.e., "critical damping"). This is a somewhat artificial situation, however, since the effort will vary in practice and the critical balance will not be maintained. For the more realistic case (c), the model tracks the simulations reasonably well.

The middle column of Fig. 6 shows that db/dt from eq. 21 (with $R(t)$ replaced by constant R), which for cases (a) and (b) is quadratic in b, agrees quite closely with the simulated differences $b(t + 1) - b(t)$. The calibration of the model is based on the variance–mean relationship $V = \phi_0 b(1 - b)$, which is compared with the simulated variance–mean relationship in the right-hand column. The agreement is quite close, especially towards the steady state, but there are some departures from the curve, and these are no doubt responsible for the discrepancies in the left-hand column.

Calibration from fine-scale effort data

Deng et al. (2005) analyzed high-polling-frequency VMS data collected every 15 min from all prawn trawl vessels entering three 6 n.mi. × 6 n.mi. grids in the Gulf of Carpentaria during two seasons. By joining consecutive polled positions, they were able to recreate the vessels' trawl tracks and, by further binning these tracks to 12 m × 12 m pixels, they obtained distributions of coverage. These distributions are shown in Fig. 7, which is based on Deng et al.'s fig. 8. It can be seen that negative binomial distributions, with parameters estimated from the empirical distributions using maximum likelihood, fit the data reasonably well. The estimated mean and β are shown in Table 1. Comparison with the spatial distributions in Deng et al.'s fig. 6 shows that the use of β to quantify aggregation makes sense, with grid C in 1998 appearing almost random ($\beta = 0.50$) and grid A in 1999 appearing highly aggregated ($\beta = 9.71$). The results also show that the amount of aggregation varies among both grids and years.

Deng et al. (2005) also assessed the effect of increasing overall effort on the pixel-scale coverage distribution by simulating pixel-scale trawl patterns by sampling actual trawl tracks recorded as GPS data. They achieved this by (*i*) sampling (without replacement) a position from the VMS data and (*ii*) sampling (with replacement) a set of daily tracks from the GPS data and overlaying these tracks so that the centroid coincided with the VMS position. The process was repeated until the desired level of total effort was reached. The resulting distributions of coverage are shown in Fig. 8, which is based on Deng et al.'s (2005) fig. 5*a*. The negative binomial distribution, though not a perfect fit, has sufficient flexibility to capture the main shape of these distributions, especially relative to the Poisson distribution. The range of β values for these simulations (Table 2) is somewhat smaller than for the real trawl patterns.

These simulations demonstrated how aggregation can arise from the combination of pixel-scale patterns in the track of a single vessel targeting a patch of prawns and of intermediate-scale clustering (due perhaps to the avoidance of features on the sea-

Fig. 6. Results of simulations for $d = 0.1$ (top row) and $d = 0.3$ (bottom row) and case (a): $r = 0.11$, $E(t) = 1$; case (b): $r = 0.3$, $E(t) = 1$; and case (c): $r = 0.11$, $E(t)$ as shown in Fig. 5. The left-hand column compares three simulations of the mean relative biomass against time (black lines) with the theoretical model (blue–grey lines), the solution of eq. 21. (For the coloured version of this figure, refer to the Web site at http://www.nrcresearchpress.com/doi/full/10.1139/cjfas-2013-0426.) The middle column compares the simulated (black lines) annual difference in mean relative biomass with the derivative dB/dt predicted by the model (blue–grey lines) for cases with constant $E(t)$. The right-hand column shows the variance of the simulated (points) relative biomass against the mean relative biomass, and overlaid is the variance–mean relationship assumed by our model (line).

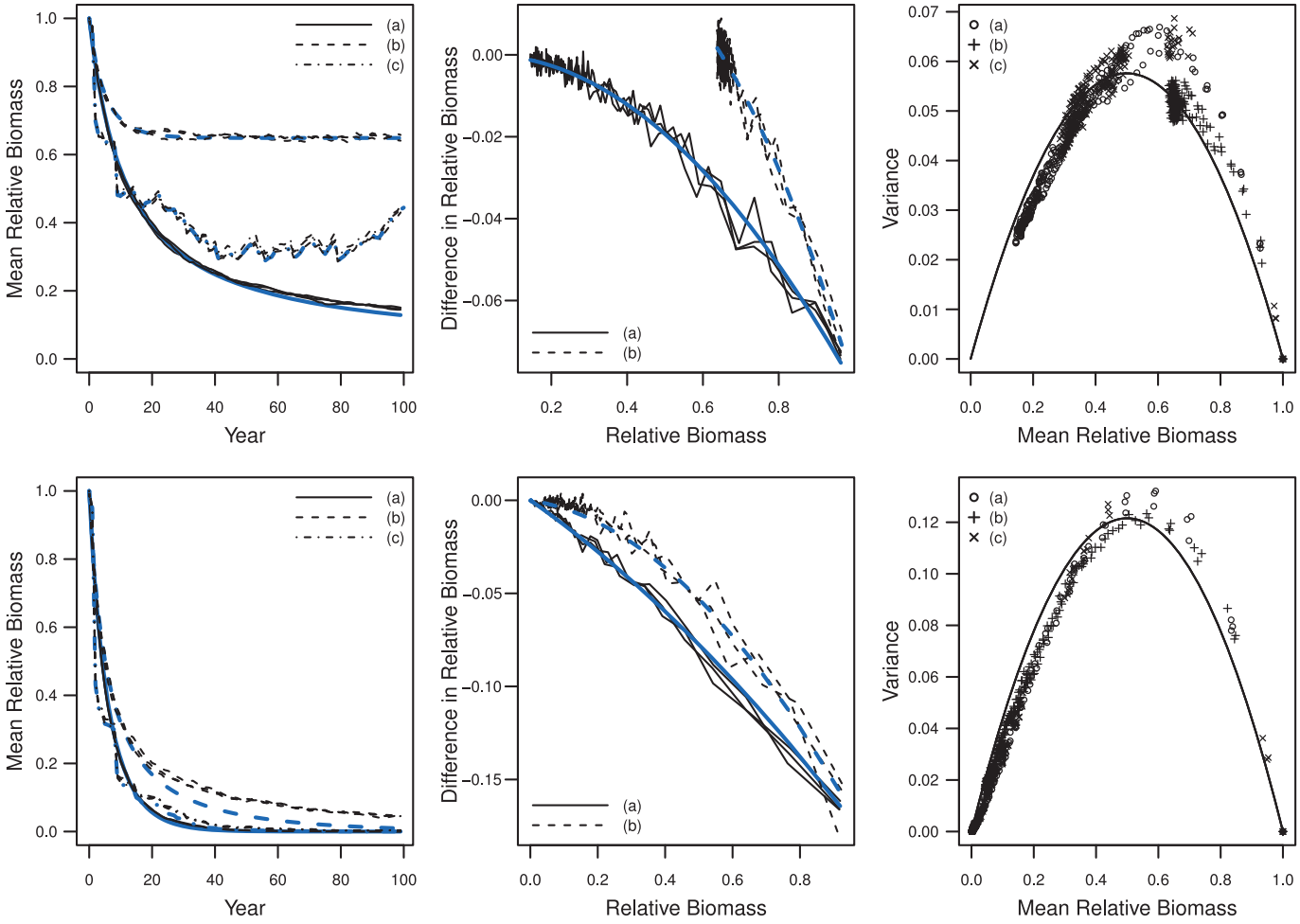

bed, such as rough bottom, an inverse hot spot). A study by Rijnsdorp et al. (1998) on beam trawling in the North Sea also found aggregation at larger scales (10 n.mi.). However, they found that the pattern within squares of sides = 1.8 km, based on smaller squares of sides = 0.18 km, was approximately random (i.e., $\beta = 0$).

Data needs for applying the model

In this section we outline the minimum data required to drive the model for the purpose of benthic impact assessment and management strategy evaluation. The model requires, for each type of fauna, values for the small-scale rates d and r and, for each management grid, values for the aggregation β, the initial pre-exploitation biomass $B(0)$, and the effort history.

The effort history must be provided from the start of the exploitation era, through to the current day and, if required, onward into the future. If the logbook record is incomplete for the early stages of a fishery, some kind of hindcasting based on auxiliary information is required. The future projection phase of the modelling would encompass proposed alternative management strategies. Projecting effort into the future in response to management actions could be based on advice from an expert panel or from detailed bioeconomic modelling.

To set β requires subgrid information on the pattern of trawling, possibly from GPS plotter tracks or from high-frequency VMS data. One could formally estimate β from the variance-to-mean ratio of subgrid coverage ($\hat{\beta}$ = variance/mean – 1) as done by Rijnsdorp et al. (1998). If the evidence suggests that trawling is random within a management grid, then one can set $\beta = 0$. In such a case the depletion due to effort E would be $1 - \exp(-dE)$, not $1-(1-d)^E$ as has been assumed (e.g., Piet et al. 2000). In the absence of subgrid data, one could use a simulation approach based on vessel behaviour as described in the section "Validation and calibration" to generate subgrid patterns from which β might be derived. Vessel behaviour could comprise hunting patterns (low β) or targeting of boils (high β).

The small-scale rate d would ideally be obtained from trawl depletion experiments that estimate per-trawl depletion rates. The small-scale rate r would be estimated from follow-up recovery monitoring extending over several years (e.g., Poiner et al. 1998; Pitcher et al. 2008). In the absence of such data, one could borrow estimates from an experiment in a similar or related study area or from meta-analyses such as Collie et al. (2000) or Kaiser et al. (2006).

Fig. 7. Histograms of coverage for the three grids (A, B, and C) studied by Deng et al. (2005) over 1998–1999. The circles are the expected percent frequencies for a negative binomial distribution fit by maximum likelihood.

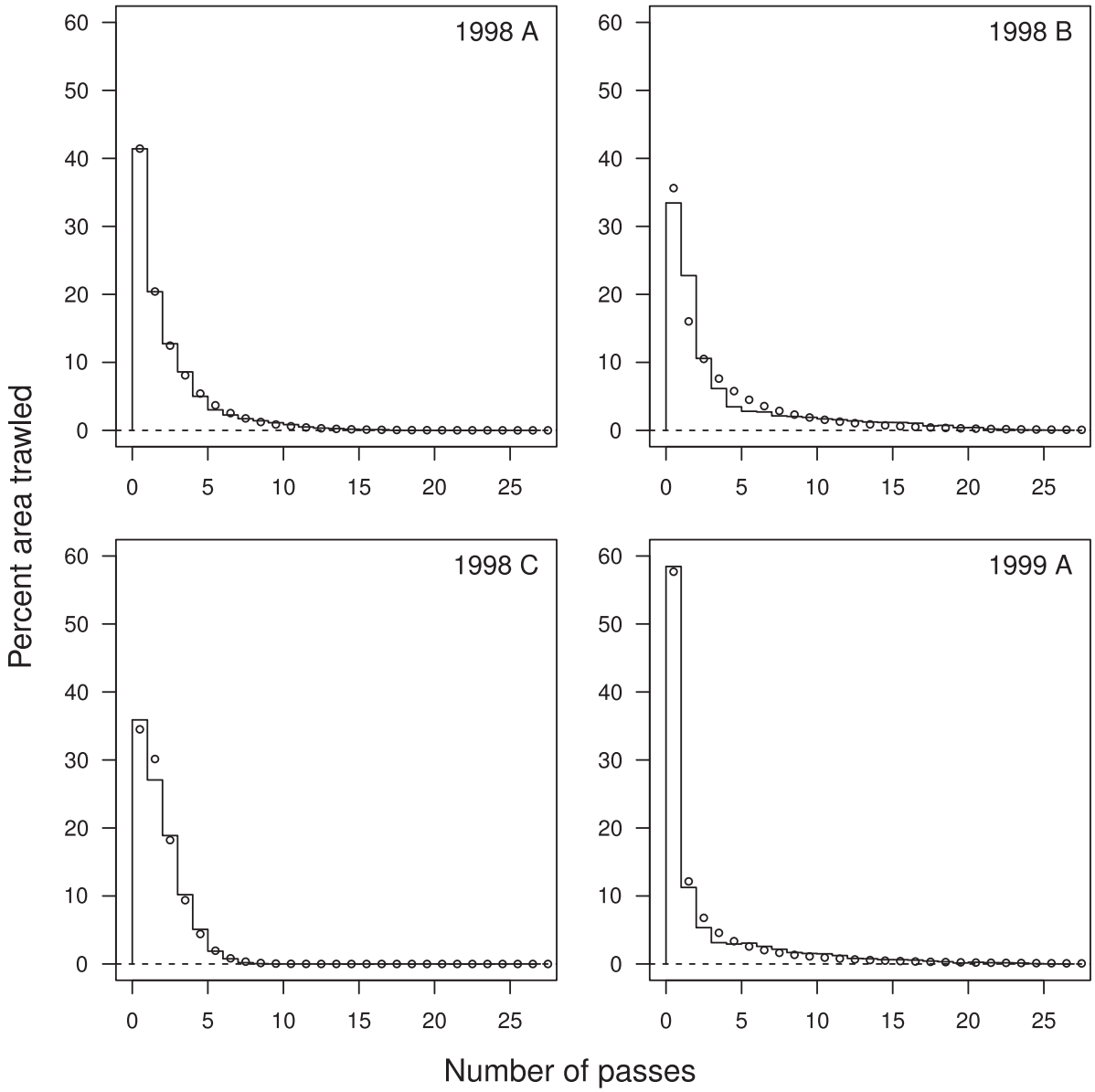

Table 1. Summary statistics of the coverage for three grids in the Gulf of Carpentaria in 1998 and 1999 studied by Deng et al. (2005).

Grid	Year	Mean	Variance	β
A	1998	1.81	6.65	2.67
A	1999	2.25	24.11	9.71
B	1998	3.25	23.47	6.22
C	1998	1.31	1.98	0.50

Note: Effort in grids B and C was too low in 1999 for meaningful analysis.

Table 2. Summary statistics for three simulated levels of effort based on the observed VMS pattern in grid A in Deng et al. (2005).

No. of tracks	Mean	Variance	β	Mean/β
100	1.53	1.97	0.29	5.32
200	3.26	6.55	1.01	3.22
400	6.34	16.00	1.53	4.15

The biomass distribution at the end of the simulation depends on the biomass distribution prior to trawling. Predictions of pristine biomass may be derived from environmental variables linked to seabed survey data, if available. In data-poor situations, however, one needs to make simplifying assumptions, the simplest assumption being that the pristine biomass is uniform, which amounts to working with relative biomass b. A fishery-scale summary, such as the mean of b over all grids, quantifies the ratio of the mean biomass to the mean pristine biomass, but only under the assumption of uniform pristine density. This assumption, therefore, causes a distortion in the real impact when the biomass distribution is correlated, either positively or negatively, with the trawling distribution, and so it is preferable to account for the pristine biomass distribution whenever possible.

Discussion

We have developed a model that estimates the grid-scale effect of trawling on different types of sessile benthic fauna from pixel-scale impact data. The model accommodates a range of trawling aggregation behaviours, as parameterized by β. Regional-scale as-

Fig. 8. Histograms of coverage for simulated fine-scale effort studied by Deng et al. (2005). The observed values are connected by lines, as in Deng et al.'s fig. 5*a*. The points are the expected percent frequencies for a negative binomial distribution fit by maximum likelihood. The expected values under a Poisson distribution for 200 tracks are denoted by the arrowheads.

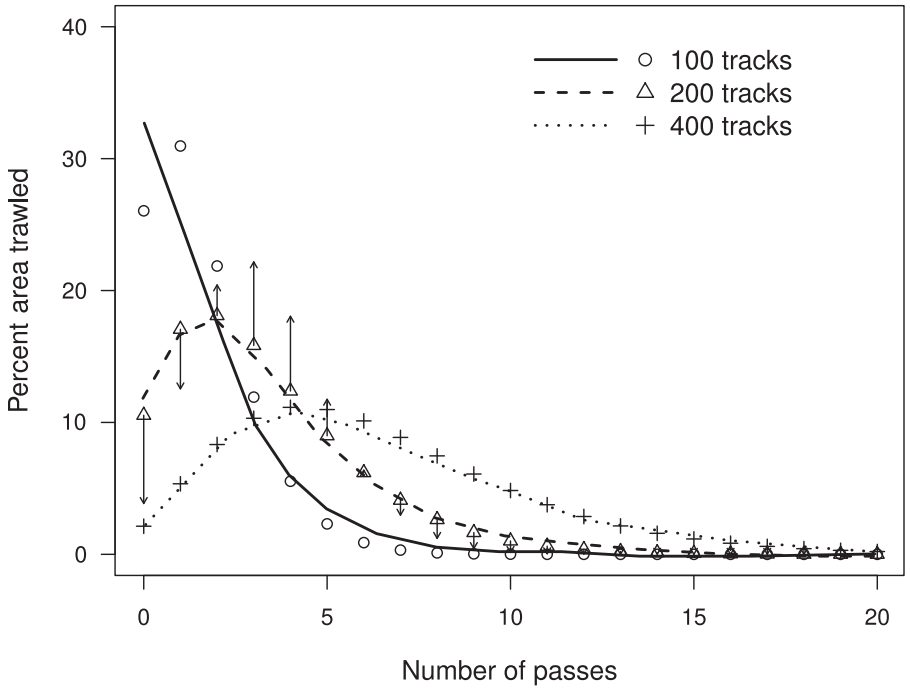

sessments of the impact of trawling can be obtained by summarizing over the grid-scale impacts.

An important finding of this work has been the relationship between processes at the pixel scale and processes at the grid scale. We have seen how rates of processes on the pixel scale (r and d), which would be the rates measured by field experiments, translate into rates of processes on the grid scale (R and D), which are the quantities of relevance to the ecosystem-based fisheries manager. Crucially, the translation from pixel to grid scale depends on the aggregation parameter β.

The model assumes that the random trawling process, though temporally aggregated, is over the long term spatially homogeneous within the grid. This assumption could be removed if information was available regarding any persistent spatial aggregation of effort within the grid. For instance, part of the grid could be untrawlable because of rough bottom, or there could be persistent aggregations of target species within the grid. This information could be accommodated by subdividing the grid and appropriately reallocating effort to the subdivisions. Hill et al. (2002) used this method to reallocate historical logbook effort on a 6 n.mi. grid to a 1 n.mi. grid, based on more recent VMS data. Their impact model was run on the finer grid with the assumption of random trawling within each grid.

Recent advances in the use of VMS (see Lee et al. 2010 and references therein) imply that fine-scale effort distributions are accessible, so that modelling of impacts into the future can benefit from this. These distributions are still likely to be at a coarser scale than gear scale, but the link to gear scale could be routinely made by assuming random trawling at the subgrid scale.

As stated in the section "Grid- and pixel-scale distribution of effort", it is also possible to specify the spatial distribution stochastically. One candidate is the hot spot mechanism, which is quite distinct from the hot time mechanism. Hot spots allow for patches that are persistently heavily trawled and for others that are persistently lightly trawled within a grid. The long-term effect is that there may be refuges of relatively low trawling within the grid in which the biomass is barely depleted; in contrast, the hot times mechanism will eventually trawl all patches of the grid because the process is spatially homogeneous. Unfortunately, the hot spot formulation does not yield a grid-scale equation like eq. 1 because the independence of biomass and trawling distributions does not hold (section "Depletion with recovery"); as far as we know, there is no alternative to calculating the history in each patch separately. However, this requirement may not be too onerous if the grid can be described by a small number of heterogeneous patches, each having random trawling within.

Adequately modelling the aggregation of trawling over time is a complex issue. The hot time mechanism proved to be a reasonable approximation for the simulation in the Supplementary Materials[1]; however, this may not always be applicable. One suggestion to distinguish the hot time and hot spot mechanisms, assuming NBD coverage, is to measure β and μ/β over time; hot time patterns would have slowly varying β, whereas hot spot patterns would have slowly varying μ/β. Our analytical method of characterizing aggregation complements the more empirical approach of Piet and Quirijns (2009). These authors analyzed the distribution of Dutch beam trawl effort in the North Sea over a range of both spatial and temporal scales. Their research has the potential to provide further insight into modelling the aggregation mechanism over time.

This method was originally developed for situations in which the biomass distributions were unknown, requiring the use of relative biomass (Ellis and Pantus 2001). Increasingly, however, species distribution models have become available. For example, Pitcher et al. (2007*a*, 2007*b*) obtained predictions of pristine biomass in the GBR and Torres Strait using generalized linear models fit to benthic survey data. These distributions were then used by Pitcher et al. (2007*a*) in the GBR and by Pantus et al. (2007) and Ellis et al. (2008) in Torres Strait as starting values for simulations under various trawl management scenarios.

One might consider how this model could be adapted for mobile species. Typically, mobile species are modelled using very coarse spatial units or even aggregated to the whole fishery (e.g., stock assessment models). This model was developed principally

for sessile species where fine-scale structure is important and for which existing models for mobile species would not be appropriate. Nevertheless, we could consider adapting the model by imagining that after each tow of area a, the biomass gets redistributed over an effective area e ($>a$). The model is modified by scaling the swept area by e/a and reducing the depletion rate by a/e. Comparison with eqs. 14 and 15 shows that this is equivalent to scaling β by a/e, which tends to make trawling less aggregated (closer to Poisson).

Of more relevance is the extension to sessile species having longer-range larval dispersal. We can obtain some qualitative insight as to how this affects the model, since longer-range dispersal should smooth the biomass across pixels. This is because dispersal from high-b (low-b) pixels will raise (lower) the biomass in low-b (high-b) pixels relative to the background rate r. This leads to a lowering of the variance V across pixels (eq. 20) and hence of ϕ, leading to a raising of R closer to small-scale rate r.

Should more information become available, the model can be improved. Areas for improvement include the following: further incorporation of stochastic depletion rates as measured by Burridge et al. (2003) — see Appendix A; relaxation of the assumption of static carrying capacity (e.g., based on monitoring of habitat quality); recovery through intergrid migration (e.g., based on hydrodynamic modelling of larval transport); benthic community interactions during recovery–depletion; and more accurate characterization of recovery by separating growth and recruitment (e.g., based on studies of recovery dynamics such as Pitcher et al. (2008)).

This model has already been used to evaluate alternative management strategies for fishery-scale impacts of trawling around the north and northeast coasts of Australia: in the GBR using prospective effort and closures scenarios (Ellis and Pantus 2001) later followed by retrospective scenarios to assess the benefit of the management actions subsequently implemented (Pitcher et al. 2007*a*; N. Ellis and C. Pitcher, unpublished data); in Torres Strait to assess potential spatial closures (Ellis et al. 2008); and in the Gulf of Carpentaria to examine the effect of effort reduction at fine scales (Hill et al. 2002) and to examine the utility of adaptive closures within habitats (Bustamante et al. 2011; Dichmont et al. 2013). Similar evaluations of closures and effect restrictions have been conducted for the North Sea using a different type of benthic production model (Hiddink et al. 2006*b*; based on Duplisea et al. 2002 and Hiddink et al. 2006*a*).

Acknowledgements

The authors thank Tony Smith, Yimin Ye, and two anonymous referees for insightful criticism that prompted us to substantially improve an early version of the paper; we also thank the three anonymous referees of this manuscript for further constructive comment. We also thank Roy Deng for providing the data used in Deng et al. (2005). We are especially grateful to the late Burke Hill for his patient and valued advice. This work was partially funded by the Great Barrier Reef Marine Park Authority, Australia, and principally funded by CSIRO's Wealth From Oceans Flagship.

References

Abramowitz, M., and Stegun, I.A. 1972. Handbook of mathematical functions with formulas, graphs, and mathematical tables. 9th printing. Dover Publishing, New York.

Bergman, M.J., and van Santbrink, J.W. 2000. Mortality in megafaunal benthic populations caused by trawl fisheries on the Dutch continental shelf in the North Sea in 1994. ICES J. Mar. Sci. **57**: 1321–1331. doi:10.1006/jmsc.2000.0917.

Burridge, C.Y., Pitcher, C.R., Wassenberg, T.J., Poiner, I.R., and Hill, B.J. 2003. Measurement of the rate of depletion of benthic fauna by prawn (shrimp) otter trawls: an experiment in the Great Barrier Reef, Australia. Fish. Res. **60**: 237–253. doi:10.1016/S0165-7836(02)00179-0.

Burridge, C.Y., Pitcher, C.R., Hill, B.J., Wassenberg, T.J., and Poiner, I.R. 2006. A comparison of demersal communities in an area closed to trawling with those in adjacent areas open to trawling: a study in the Great Barrier Reef Marine Park, Australia. Fish. Res. **79**(1–2): 64–74. doi:10.1016/j.fishres.2005.11.025.

Bustamante, R.H., Dichmont, C., Ellis, N., Griffiths, S., Rochester, W.A., Burford, M., Rothlisberg, P., Dell, Q., Tonks, M., Lozano-Montes, H., Deng, R., Revill, A., Van Der Velde, T., Moeseneder, C., Cheers, S., Donovan, A., Fry, G., Tickell, S., Pascual, R., Smith, F., and Morello, B. 2011. Effects of trawling on the benthos and biodiversity: development and delivery of a spatially-explicit management framework for the Northern Prawn Fishery. Final Report to the Project FRDC 2005, CSIRO Marine and Atmospheric Research.

Collie, J.S., Escanero, G.A., and Valentine, P.C. 1997. Effects of bottom fishing on the benthic megafauna of Georges Bank. Mar. Ecol. Prog. Ser. **155**: 159–172. doi:10.3354/meps155159.

Collie, J.S., Hall, S.J., Kaiser, M.J., and Poiner, I.R. 2000. A quantitative analysis of fishing impacts on shelf-sea benthos. J. Anim. Ecol. **69**: 785–798. doi:10.1046/j.1365-2656.2000.00434.x.

Cox, D.R., and Isham, V. 1980. Point processes. Chapman & Hall, London.

Deng, R., Dichmont, C., Milton, D., Haywood, M., Vance, D., Hall, N., and Die, D. 2005. Can vessel monitoring system data also be used to study trawling intensity and population depletion? The example of Australia's northern prawn fishery. Can. J. Fish. Aquat. Sci. **62**(3): 611–622. doi:10.1139/f04-219.

Dichmont, C.M., Ellis, N., Bustamante, R.H., Deng, R., Tickell, S., Pascual, R., Lozano-Montes, H., and Griffiths, S. 2013. Evaluating marine spatial closures with conflicting fisheries and conservation objectives. J. Appl. Ecol. **50**(4): 1060–1070. doi:10.1111/1365-2664.12110.

Diggle, P.J., and Milne, R.K. 1983. Negative binomial quadrat counts and point processes. Scand. J. Stat. **10**: 257–267.

Duplisea, D.E., Jennings, S., Warr, K.J., and Dinmore, T.A. 2002. A size-based model of the impacts of bottom trawling on benthic community structure. Can. J. Fish. Aquat. Sci. **59**(11): 1785–1795. doi:10.1139/f02-148.

Eaton, W.W., and Fortin, A. 1978. A third interpretation for the generating process of the negative binomial distribution. Am. Soc. Rev. **43**: 264–267. doi:10.2307/2094703.

Ellis, N., and Pantus, F. 2001. Management Strategy Modelling: Tools to evaluate trawl management strategies with respect to impacts on benthic biota within the Great Barrier Reef Marine Park area [online]. CSIRO Marine Research, Cleveland, Australia. Available from http://www.cmar.csiro.au/e-print/open/ellisn_2001.pdf.

Ellis, N., Pantus, F., Welna, A., and Butler, A. 2008. Evaluating ecosystem-based management options: effects of trawling in Torres Strait, Australia, in Marine resources, biophysical processes, and environmental management of a tropical shelf seaway: Torres Strait, Australia. Continental Shelf Res. **28**: 2324–2338. doi:10.1016/j.csr.2008.03.031.

Gurland, J. 1959. Some applications of the negative binomial and other contagious distributions. Am. J. Public Health, **49**(10): 1388–1399. doi:10.2105/AJPH.49.10.1388.

Hansson, M., Lindegarth, M., Valentinsson, D., and Ulmestrand, M. 2000. Effects of shrimp-trawling on abundance of benthic macrofauna in Gullmarsfjorden, Sweden. Mar. Ecol. Prog. Ser. **198**: 191–201. doi:10.3354/meps198191.

Hiddink, J.G., Hutton, T., Jennings, S., and Kaiser, M.J. 2006*a*. Predicting the effects of area closures and fishing effort restrictions on the production, biomass, and species richness of benthic invertebrate communities. ICES J. Mar. Sci. **63**: 822–830. doi:10.1016/j.icesjms.2006.02.006.

Hiddink, J.G., Jennings, S., Kaiser, M.J., Queirós, A.M., Duplisea, D.E., and Piet, G.J. 2006*b*. Cumulative impacts of seabed trawl disturbance on benthic biomass, production, and species richness in different habitats. Can. J. Fish. Aquat. Sci. **63**(4): 721–736. doi:10.1139/f05-266.

Hill, B.J., Haywood, M., Venables, B., Gordon, S., Condie, S., Ellis, N., Tyre, D., Vance, D., Mansbridge, J., Dunn, J., Moeseneder, C., Bustamante, R., and Pantus, F. 2002. Final Report on FRDC Project 2000/160: Surrogates I — Predictors, impacts, management and conservation of the benthic biodiversity of the Northern Prawn Fishery. CSIRO, Cleveland.

Jennings, S., and Kaiser, M.J. 1998. The effects of fishing on marine ecosystems. Adv. Mar. Biol. **34**: 201–352. doi:10.1016/S0065-2881(08)60212-6.

Kaiser, M.J., Edwards, D.B., Armstrong, P.J., Radford, K., Lough, N.E.L., Flatt, R.P., and Jones, H.D. 1998. Changes in megafaunal benthic communities in different habitats after trawling disturbance. ICES J. Mar. Sci. **55**(3): 353–361. doi:10.1006/jmsc.1997.0322.

Kaiser, M.J., Collie, J.S., Hall, S.J., Jennings, S., and Poiner, I.R. 2002. Modification of marine habitats by trawling activities: prognosis and solutions. Fish Fish. **3**: 114–136. doi:10.1046/j.1467-2979.2002.00079.x.

Kaiser, M.J., Clarke, K.R., Hinz, H., Austen, M.C.V., Somerfield, P.J., and Karakassis, I. 2006. Global analysis of response and recovery of benthic biota to fishing. Mar. Ecol. Prog. Ser. **311**: 1–14. doi:10.3354/meps311001.

Kenchington, E.L., Gilkinson, K.D., MacIsaac, K.G., Bourbonnais-Boyce, C., Kenchington, T.J., Smith, S.J., and Gordon, D.C. 2006. Effects of experimental otter trawling on benthic assemblages on Western Bank, northwest Atlantic Ocean. J. Sea Res. **56**(3): 249–270. doi:10.1016/j.seares.2006.03.010.

Lee, J., South, A.B., and Jennings, S. 2010. Developing reliable, repeatable, and accessible methods to provide high-resolution estimates of fishing-effort distributions from vessel monitoring system (VMS) data. ICES J. Mar. Sci. **67**(6): 1260–1271. doi:10.1093/icesjms/fsq010.

McConnaughey, R.A., Mier, K.L., and Dew, C.B. 2000. An examination of chronic

trawling effects on soft-bottom benthos of the eastern Bering Sea. ICES J. Mar. Sci. **57**(5): 1377–1388. doi:10.1006/jmsc.2000.0906.

Moran, M.J., and Stephenson, P.C. 2000. Effects of otter trawling on macrobenthos and management of demersal scalefish fisheries on the continental shelf of north-western Australia. ICES J. Mar. Sci. **57**(3): 510–516. doi:10.1006/jmsc.2000.0718.

Pantus, F., Ellis, N., Browne, M., Okey, T., Robinson, M., Rochester, W., and Welna, A. 2007. Torres Strait management scenario evaluation: effects of trawling. Report on CRC Torres Strait task T3.3. CSIRO, Cleveland. ISBN: 978-1-921232-90-9.

Piet, G.J., and Quirijns, F.J. 2009. The importance of scale for fishing impact estimations. Can. J. Fish. Aquat. Sci. **66**(5): 829–835. doi:10.1139/F09-042.

Piet, G.J., Rijnsdorp, A.D., Bergman, M.J., van Santbrink, J.W., Craeymeersch, J., and Buijs, J. 2000. A quantitative evaluation of the impact of beam trawling on benthic fauna in the southern North Sea. ICES J. Mar. Sci. **57**: 1332–1339. doi:10.1006/jmsc.2000.0915.

Pitcher, C.R., Poiner, I.R., Hill, B.J., and Burridge, C.Y. 2000. Implications of the effects of trawling on sessile megazoobenthos on a tropical shelf in north-eastern Australia. ICES J. Mar. Sci. **57**: 1359–1368. doi:10.1006/jmsc.2000.0911.

Pitcher, C.R., Doherty, P., Arnold, P., Hooper, J., Gribble, N., Bartlett, C., Browne, M., Campbell, N., Cannard, T., Cappo, M., Carini, G., Chalmers, S., Cheers, S., Chetwynd, D., Colefax, A., Coles, R., Cook, S., Davie, P., De'ath, G., Devereux, D., Done, B., Donovan, T., Ehrke, B., Ellis, N., Ericson, G., Fellegara, I., Forcey, K., Furey, M., Gledhill, D., Good, N., Gordon, S., Haywood, M., Jacobsen, I., Johnson, J., Jones, M., Kinninmoth, S., Kistle, S., Last, P., Leite, A., Marks, S., McLeod, I., Oczkowicz, S., Rose, C., Seabright, D., Sheils, J., Sherlock, M., Skelton, P., Smith, D., Smith, G., Speare, P., Stowar, M., Strickland, C., Sutcliffe, P., Van der Geest, C., Venables, W., Walsh, C., Wassenberg, T., Welna, A., and Yearsley, G. 2007*a*. Seabed Biodiversity on the Continental Shelf of the Great Barrier Reef World Heritage Area. AIMS/CSIRO/QM/QDPI CRC Reef Research Task Final Report.

Pitcher, C.R., Haywood, M., Hooper, J., Coles, R., Bartlett, C., Browne, M., Cannard, T., Carini, G., Carter, A., Cheers, S., Chetwynd, D., Colefax, A., Cook, S., Davie, P., Ellis, N., Fellegara, I., Forcey, K., Furey, M., Gledhill, D., Hendriks, P., Jacobsen, I., Johnson, J., Jones, M., Last, P., Marks, S., McLeod, I., Sheils, J., Sheppard, J., Smith, G., Strickland, C., Van der Geest, C., Venables, W., Wassenberg, T., and Yearsley, G. 2007*b*. Mapping and Characterisation of Key Biotic & Physical Attributes of the Torres Strait Ecosystem. CSIRO/QM/QDPI CRC Torres Strait Task Final Report.

Pitcher, C.R., Austin, M., Burridge, C.Y., Bustamante, R.H., Cheers, S.J., Ellis, N., Jones, P.N., Koutsoukos, A.G., Moeseneder, C.H., Smith, G.P., Venables, W., and Wassenberg, T.J. 2008. Recovery of seabed habitat from the impact of prawn trawling in the far northern section of the Great Barrier Reef Marine Park. CSIRO Final Report to GBRMPA, CSIRO Division of Marine Research, Cleveland.

Pitcher, C.R., Burridge, C.Y., Wassenberg, T.J., Hill, B.J., and Poiner, I.R. 2009. A large scale BACI Experiment to test the effects of prawn trawling on seabed biota in a closed area of the Great Barrier Reef Marine Park, Australia. Fish. Res. **99**(3): 168–183. doi:10.1016/j.fishres.2009.05.017.

Poiner, I., Glaister, J., Pitcher, R., Burridge, C., Wassenberg, T., Gribble, N., Hill, B., Blaber, S., Milton, D., Brewer, D., and Ellis, N. 1998. Environmental effects of prawn trawling in the far northern section of the Great Barrier Reef: 1991–1996. Final Report to the Great Barrier Reef Marine Park Authority and Fisheries Research and Development Corporation.

Quenouille, M.H. 1949. A relation between the logarithmic, Poisson, and negative binomial series. Biometrics, **5**: 162–164. doi:10.2307/3001917. PMID: 18151958.

Rijnsdorp, A.D., Buys, A.M., Storbeck, F., and Visser, E.G. 1998. Micro-scale distribution of beam trawl effort in the southern North Sea between 1993 and 1996 in relation to the trawling frequency of the sea bed and the impact on benthic organisms. ICES J. Mar. Sci. **55**: 403–419. doi:10.1006/jmsc.1997.0326.

Rijnsdorp, A.D., Poos, J.J., and Quirijns, F.J. 2011. Spatial dimension and exploitation dynamics of local fishing grounds by fishers targeting several flatfish species. Can. J. Fish. Aquat. Sci. **68**(6): 1064–1076. doi:10.1139/f2011-032.

Sainsbury, K.J., Campbell, R.A., and Whitelaw, A.W. 1992. Effects of trawling on the marine habitat on the North West Shelf of Australia and implications for sustainable fisheries management. *In* Sustainable fisheries through sustaining fish habitat. *Edited by* D.A. Hancock. Aust. Soc. Biol. Workshop. Australian Government Publishing Service, Canberra. pp. 137–145.

Sainsbury, K.J., Campbell, R.A., Lindholm, R., and Whitelaw, A.W. 1997. Experimental management of an Australian multispecies fishery: examining the possibility of trawl-induced habitat modification. *Edited by* E.K. Pikitch, D.D. Huppert, and M.P. Sissenwine. Global trends: fisheries management. American Fisheries Society, Bethesda, Md. pp. 107–112.

Schaefer, M.B. 1954. Some aspects of the dynamics of populations important to the management of commercial marine fisheries. Bull. Int.-Am. Trop. Tuna Comm. **1**: 27–56. doi:10.1007/BF02464432.

Tuck, I.D., Hall, S.J., Robertson, M.R., Armstrong, E., and Basford, D.J. 1998. Effects of physical trawling disturbance in a previously unfished sheltered Scottish sea loch. Mar. Ecol. Prog. Ser. **162**: 227–242. doi:10.3354/meps162227.

van Dolah, R.F., Wendt, P.H., and Nicholson, N. 1987. Effects of a research trawl on a hard-bottom assemblage of sponges and corals. Fish. Res. **5**(1): 39–54. doi:10.1016/0165-7836(87)90014-2.

Venables, W.N., and Ripley, B.D. 2002. Modern applied statistics with S. Springer, New York.

Appendix A. Variable depletion rate

If the depletion rate d is a random variable with probability density function $\pi(d)$, then eq. 12 becomes an integral over d:

$$\text{(A.1)}\qquad \mathbf{E}[B(t)] = \mathbf{E}[B(0)]\int_0^1 \pi(d)\sum_{k=0}^{\infty}(1-d)^k P_t(k)\,\mathrm{d}d$$

If $\pi(d)$ is a Beta distribution with parameters a and b (having mean $\overline{d} = a/(a+b)$ and variance $\overline{d}(1-\overline{d})/(a+b+1)$), then

$$\text{(A.2)}\qquad \mathbf{E}[B(t)] = \mathbf{E}[B(0)]\sum_{k=0}^{\infty}\frac{\mathrm{Beta}(b+k,a)P_t(k)}{\mathrm{Beta}(b,a)}$$

where the Beta function is defined in section 6.2 of Abramowitz and Stegun (1972). If, in addition, the coverage distribution is Poisson with mean μ, then

$$\text{(A.3)}\qquad \begin{aligned}\mathbf{E}[B(t)] &= \mathbf{E}[B(0)]\sum_{k=0}^{\infty}\frac{\mathrm{Beta}(b+k,a)\,\mathrm{e}^{-\mu}\mu^k}{\mathrm{Beta}(b,a)k!}\\ &= \mathrm{e}^{-\mu}M(b,a+b,\mu) = M(a,a+b,-\mu)\end{aligned}$$

where M is the Kummer function (Abramowitz and Stegun 1972, section 13.1.2). Numerical experiments suggest that $\mathbf{E}[B(t)]$ is a minimum in the limit $a, b \to \infty$ (i.e., when d is fixed).

Appendix B. Time-varying aggregation

A natural extension of the simple negative binomial model is to allow β to vary in time. The pgf then becomes

$$\text{(B.1)}\qquad g_t(z) = \exp\left\{-\int_0^t \frac{\log[1+\beta(s)(1-z)]E(s)\mathrm{d}s}{\beta(s)}\right\}$$

This is a generalization of eq. 3.5 in Cox and Isham (1980) to time-varying compound Poisson processes. The expression for biomass is then

$$\text{(B.2)}\qquad B(t) = \exp\left[-\int_0^t D(s)E(s)\mathrm{d}s\right]B(0)$$

where D is still given by eq. 15, but with β now a function of time. The distribution of coverage corresponding to this pgf is no longer a negative binomial, but rather some mixture of negative binomial distributions. However, the differential equation for $B(t)$ remains unchanged:

$$\text{(B.3)}\qquad \frac{\mathrm{d}B}{\mathrm{d}t} = -D(t)E(t)B(t)$$

Appendix C. Steady-state approximation for *R*

Since ϕ_0 is constant, it follows that R is also constant. To evaluate R, consider a system subject to a constant rate of effort $\overline{E}$. By evaluating expressions for steady-state biomass from the grid-scale equation (involving R) and from the pixel-scale process (involving r), the relationship between R and r is found.

The grid-scale steady-state biomass $\overline{b}^{(\mathrm{ss})}$ for this system is found by setting the left-hand side of eq. 21 to zero and solving for $\overline{b}$. This gives

$$\text{(C.1)}\qquad \bar{b}^{(ss)} = \begin{cases} 0, & \bar{E} \geq R/D \\ 1 - D\bar{E}/R, & \bar{E} < R/D \end{cases}$$

that is, either the biomass goes extinct when the effort is above a certain threshold, or it goes to a reduced level where depletion and recovery balance out. We assume $\bar{E} < R/D$ so that $\bar{b}^{(ss)} > 0$.

At the pixel scale, consider again eq. 17 giving the relative biomass at time $t + \Delta t$ in terms of the biomass at time t. Then, taking the expectation over all pixels of the logarithm of both sides of this equation yields

$$\text{(C.2)}\qquad \mathbf{E}[\log b(t + \Delta t)] = \mathbf{E}[\log b(t)] + r\Delta t(1 - \mathbf{E}[b(t)]) + \mathbf{E}[n(\Delta t)]\log(1 - d) + O(\Delta t^2)$$

By stationarity, the expectations of b are independent of t; therefore, the first two terms cancel. Also, $\mathbf{E}[n(\Delta t)] = \bar{E}\Delta t$, so that, after rearranging

$$\text{(C.3)}\qquad \mathbf{E}[b] = 1 + \bar{E}\log(1 - d)/r$$

Since $\bar{b}^{(ss)}$ and $\mathbf{E}[b]$ are the same, we may equate the right-hand sides of eqs. C.1 and C.3 to find that, after substituting for D from eq. 15:

$$\text{(C.4)}\qquad R = r\log(1 + \beta d)/[-\beta\log(1 - d)]$$

This expression is independent of $\bar{E}$.